Towards simulation at picometer-scale resolution: Revisiting inversion domain boundaries in GaN

Frédéric Lançon,[*] Luigi Genovese, and Joël Eymery

Univ. Grenoble Alpes, CEA, INAC-MEM, L_Sim, F-38054 Grenoble, France

Motivated by recent high resolution results on the inversion domain boundaries (IDB) in gallium nitride, we refine by *ab initio* DFT calculations the well established atomic model IDB* derived by Northrup *et al.* This allows us to recover these experimental results obtained by coherent x-ray diffraction and showing small additional shifts of the polarity domains, in particular 8 pm shift along the hexagonal direction. The influence of boundary conditions and electrostatic fields (IDB-IDB and IDB-surface interactions) on the results and the existence of metastable solutions is carefully discussed to stress the accuracy of the method. These results demonstrate a cross-talk between advanced characterization tools and state-of-the-art *ab initio* calculations that opens perspectives for the structural analysis of defects in the picometer range.

I. INTRODUCTION

Precision in DFT calculations for solid-state physics has been recently studied [1] and a very good reproducibility of the results has been reported among several current codes. For instance, a reproducibility of 1 pm has been found on the different calculated lattice parameters of silicon. Yet, this precision obtained in the calculation corresponds to an accuracy of 6 pm with respect to the experimental value [1]. We intend here to get a better agreement in the accuracy of geometrical characteristics of gallium nitride, a widely studied compound of technological importance. Challenged by recent experimental results [2] on very common planar defects in GaN material, we have conducted a detailed analysis of them. Gallium-nitride crystal is a wurtzitelike structure, i.e., a hexagonal lattice with one fourth of the Ga-N bonds oriented along the hexagonal-symmetry axis. Inversion domain boundaries (IDB) are interfaces between crystalline polarity domains, which can be noted $-c$ and $+c$. These domains have their hexagonal axis in common but have opposite orientations for their Ga-N bonds parallel to it. By convention, in $+c$ domains these Ga $\rightarrow$ N bonds are oriented along $[0\,0\,0\,1]$ of the material, while it is $[0\,0\,0\,\bar{1}]$ for $-c$ domains. Depending on the experimental conditions, a given type of domain is usually preferably produced during the crystal growth. The growing surface perpendicular to $[0\,0\,0\,1]$ is either Ga terminated for $+c$ domains or N terminated for $-c$. However, both domain types separated by IDB frequently coexist in thin films [3–7] and in wires [8,9]. It usually corresponds to detrimental defects in the materials, but periodic alternation of domains is garnering interest in a wide range of devices such as those for nonlinear frequency conversion [10–12].

IDB structures are usually studied by electron microscopy [3–5,7,9,13]. These studies confirm the pioneering model for IDB* introduced by Northrup *et al.* [14], who determined its structure and stability with *ab initio* DFT calculations. This model gets the lowest energy of possible structures by keeping hetero-first-neighbor bonds at the cost of some bond-angle distortions at the boundary.

It provides a characteristic shift of the Ga atomic layers by $c/8$ along the $[0\,0\,0\,1]$ direction, which is measured by high resolution transmission electron microscopy [4,7]. Indeed, electron microscopy enhances the contrast of the heavier Ga atoms with respect to the lighter N atoms. The IDB have been shown to emit light [15,16] and the emission properties of the IDB* structure have been calculated, again by DFT calculation [17], confirming its theoretical basis.

However, experimental advances are now pushing the structure characterizations of boundaries toward the "picoscopic"-scale description of condensed matter [2,18] and this can challenge the actual IDB* model. In particular, by considering IDB buried in large and long GaN rods obtained by MOVPE (metal-organic vapor phase epitaxy), Labat *et al.* [2] found an extra shift of 8 pm $\pm$ 1 pm to the $c/8$ shift of the Ga atomic layers crossing the IDB* from the $-c$ domain to the $+c$ one. The authors suggested a segregation of silicon atoms at the interface as a possible explanation of this apparent discrepancy with respect to the usual model of the IDB. Thus it is worth checking in details this model to exclude such possible external explanations of discrepancies. Previous DFT calculation of the GaN IDB* in Ref. [17] gives a hint that this accuracy is achievable, since the deviations of the calculated lattice parameters are there $\Delta a = -2.8\,\mathrm{pm}$ (-0.9%) and $\Delta c = -4.7\,\mathrm{pm}$ (-0.9%) compared to the experimental results of Ref. [19]. In this paper, we revisit the IDB* model by new *ab initio* calculations with a larger number of atoms and high energy precision. It will provide a special focus on these new accurate experimental results and allow discussing the intrinsic effect of the IDB with respect to doping distortions.

II. SETUP

Taking into account the electronic density in its ground state, DFT codes are now well established tools to calculate

---

*Frederic.Lancon@cea.fr

atomic properties for an increasing number of materials [1,20]. We have used BigDFT code [21,22], which has the particularity of expressing the electronic wave functions with a basis set of localized wavelet functions. This type of basis enables a strong compression of the data, a systematic control of the precision, and an excellent efficiency for parallel calculations. Besides, the code can take into account a variety of boundary conditions [23], from isolated molecules to periodic crystals. In particular here, this feature allows us to explore systems with either full periodic boundary conditions or free boundary conditions at the surfaces parallel to the IDB. The first case is usual for such calculations and was indeed the case for the previous calculations with 32 atoms in the supercell [14] or 48 atoms [17]. However in this case, an even number of IDB has to be introduced in the supercell, usually two IDB and two crystalline grains. In the second case, studies with free surfaces parallel to an interface are usually done with full periodic conditions while inserting a vacuum layer between the surfaces [20,24]. The width of the vacuum must minimize as much as possible the interaction through the empty space of the atoms at the surfaces. Instead, here we have used real free boundary conditions perpendicular to the IDB, while keeping periodic conditions in the two other directions. This feature is possible with the Poisson solver included in BigDFT code [23]. For both types of calculations, fully periodic or with free boundary conditions, 32 to 256 atoms have been considered. A higher focus has been given to the 80 and 128 atom systems to explore their properties.

Hartwigsen-Goedecker-Hutter pseudopotentials [25,26] (HGH) are used to simulate the interaction of the nucleus and the core electrons with the valence electrons (respectively, three and five electrons per Ga and N atom here). Calculations are done with Perdew-Burke-Ernzerhof (PBE) exchange correlation functional [27], which is a standard choice for solid-state studies and in particular is suitable for the GaN compounds [28]. The description of the wave functions, and thus the calculation precision, can be systematically improved by decreasing h_{grid}, the real-space grid spacing between the wavelet-function centers. Reasonable values of h_{grid} must be lower than twice the length parameters of the HGH pseudopotentials [29]. To go further, we have tested the convergence versus h_{grid} of the energy difference, ΔE_{zb-w}, between the zinc-blende and the wurtzite gallium-nitride crystals. The calculated limit at low h_{grid} of this quantity is $\Delta E_{zb-w} = 6.73$ meV per atom (see Fig. S2 in the Supplemental Material [30]). In this work, a value $h_{grid} = 0.02$ nm has been chosen (or lower to be commensurate with the supercell box). It corresponds to a deviation of 0.5 meV/atom on ΔE_{zb-w}.

To study the convergence of the calculations with the k-point grid, the energy of the orthogonal cell of the GaN wurtzite crystal has been calculated with an increasing number of k points up to $17 \times 10 \times 10$ (see Fig. S1 in the Supplemental Material [30]). The internal parameter u of the unit cell has been determined for each calculation. Compared to the thinnest $17 \times 10 \times 10$ mesh, a $9 \times 5 \times 5$ Monkhorst Pack mesh gives a discrepancy better than 3×10^{-5} eV/atom. This k-point grid is taken as the reference in this paper.

The computed cell parameters are: $a = 317.9$ pm, $c = 518.0$ pm, and $u = 0.377$, i.e., 195.3 pm for the Ga-N bonds parallel to [0 0 0 1] (see details in Fig. S3 in the
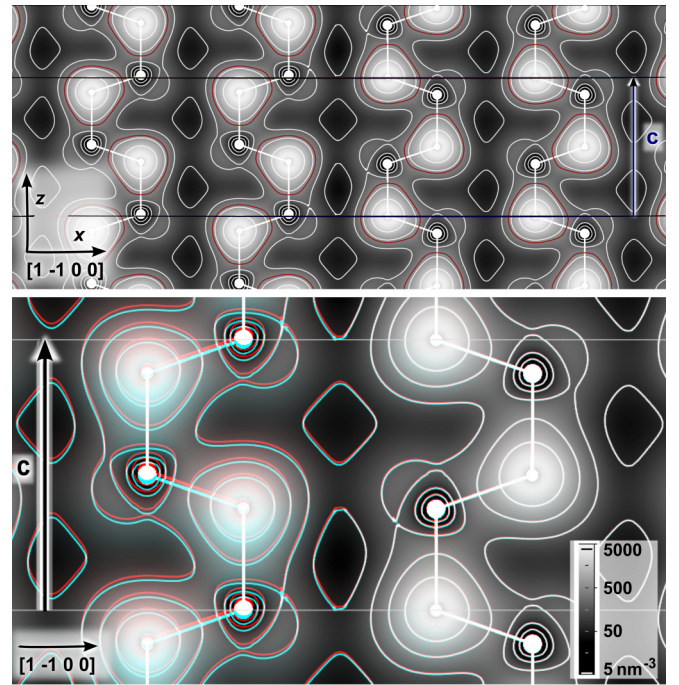

FIG. 1. Density plot of the valence-electron density at the inversion domain boundary between $+c$ and $-c$ domains (respectively, at left and right). In the Supplemental Material [30], Fig. S7 shows the plane location of the density cross section. White and black represent, respectively, the highest and the lowest electron density. Valence electrons are mostly located around nitrogen atoms. *Top:* Density of the ground state. Low and high density regions are separated by the red curves that are the isovalue lines corresponding to the average density $N_e/V = 353$ nm^{-3}, where N_e is the total number of valence electrons in the supercell of volume V. *Bottom:* The stable and the metastable structures are both shown, respectively, as red and cyan images added together. Where densities are similar, added red and cyan give white, gray, or black. The difference of density distributions and the shift of the $+c$ domains are therefore highlighted by the red color coming from the stable configuration and the cyan color coming from the metastable one. For the overlaying, the two $-c$ domains coincide far from the interface, giving them a common origin. The lattice parameter **c** is indicated and its modulus equal to 518 pm gives the scale.

Supplemental Material [30]). The agreement is excellent with the experimental determination of Ref. [19] with deviations $\Delta a = -0.9$ pm and $\Delta c = -0.6$ pm. This confirms the validity of the approach to get IDB geometry at a picometer resolution.

The IDB* are perpendicular to the b axis. In the calculations a number of unit cells are packed along b on each side of the interface, and a $9 \times 1 \times 5$ mesh of k points is then sufficient. The crystalline grains are thus spanning the b direction, which is taken as our x axis and is equal to $[1\,\bar{1}\,0\,0]$ in hexagonal notation. The y axis corresponds to $[1\,1\,\bar{2}\,0]$ (a axis) and the z axis to $[0\,0\,0\,1]$ (c axis).

III. RESULTS

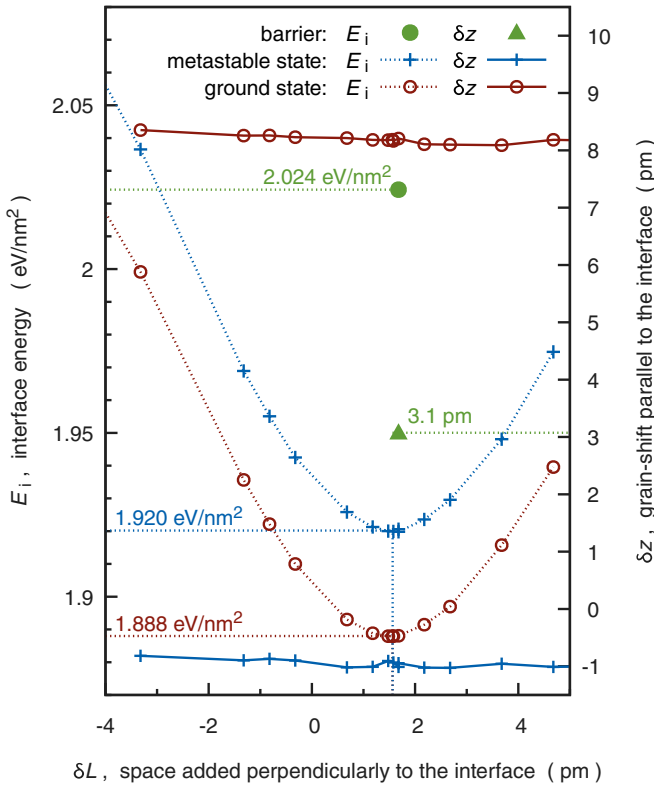Two atomic configurations have been considered as starting structures for minimizing the system energy. First, the

FIG. 2. Interface energy E_i (dashed lines and left axis) and domain shift δz along $[0\,0\,0\,1]$ (solid lines and right axis) versus spacing δL perpendicular to the interfaces. δL is the initial deviation at the interface of the interplanar distance $d_{1\bar{1}0\,0}$. Periodic boundary conditions have been used and data correspond to a 80 atom configuration. In such a periodic system with 2 IDB, the interface energy E_i is, per surface unit, half the difference between the total potential energy of the configuration and the energy of a crystalline configuration with the same number of atoms. Domain shifts $\delta z = z_{Ga} - z_N$ are calculated as coordinate differences between central Ga atoms of the $+c$ domain and central nitrogen atoms of the facing layer in the $-c$ domain (see Fig. 4 in the appendix). Filled circle and triangle correspond, respectively, to E_i and Δz for the barrier between the two minima.

structure as described by Northrup *et al.* [14] where the Ga layers perpendicular to the $[0\,0\,0\,1]$ direction in one grain are aligned with nitrogen layers in the second grain. Second, a similar configuration except that an extra shift $\delta z = 8$ pm is added between the $+c$ and $-c$ domains. This particular value of δz corresponds to the experimental results of Ref. [2]. These setups have been used for systems with increasing grain sizes along x up to a total of 256 atoms, i.e., 64 $(1\,\bar{1}0\,0)$ layers in each grain. For all grain sizes and after energy minimization, the lowest energy has always been obtained when the initial shift is 8 pm. The final optimum shift is $\delta z = 8.2 \pm 0.1$ pm in agreement with the Bragg imaging results [2] obtained by coherent x-ray diffraction (see Figs. 4 and 5 in the appendix). A metastable state is reached by the configurations without initial shift. Its final grain shift corresponds actually to a negative shift $\delta z = -1.0 \pm 0.1$ pm. Other configurations with intermediate initial grain shifts have also been tested and all of them have fallen in one or the other of these two minima.

Figure 1 shows the structure and electron density of the IDB for both states in an overlay mode to appreciate the very small change between them (see also Figs. S6 to S8 in the Supplemental Material [30]). It evidences how big the challenge is to measure it experimentally. Interferometric approaches, such as coherent x-ray diffraction and electron holography, seem indeed well suited to get these small variations in atomic structures.

Each calculation has been performed at constant supercell sizes and, in particular along y and z, the a and c lattice parameters have been set to the perfect crystal parameters to mimic infinitely-separated interfaces. However, fixed size along x forbids free grain shifts perpendicular to the interface. Therefore, the grain separation at the interface may not be the optimum distance. Thus different configurations have been constructed with different shifts δL by adding or removing space between the domains ($\delta L = 0$ corresponding to the direct inversion of half of the bulk structure when creating the IDB). These configurations have been relaxed with the above protocol. Figure 2 shows the interface energy E_i versus δL. For both stable and metastable states, and for all grain sizes studied, we found that the optimal values are $\delta L < 2$ pm. However, because of long range interactions between the two interfaces of the periodic configurations, the bulk part of the crystals may be strained. At the energy minimum, a careful analysis of this strain gives a value of $\varepsilon_{xx} = +4 \times 10^{-4}$ for the 80 atom configuration whose distance between interfaces is 2.75 nm. Thus the IDB-IDB interaction is repulsive and its effect on the lattice deformation is small for this size. Nevertheless, for the grain shift perpendicular to the IDB, the uncertainty is mainly due to this strain effect. In the value of δL, the share of the elastic expansion ε_{xx} on one hand, and that of the optimal shift δx at the IDB on the other hand, are discussed below in the analysis of the boundary-condition effects.

The formation energy E_i of the most stable IDB structure is 1.89 eV/nm^2, while for the metastable state it is 1.92 eV/nm^2. Considering the differences in the DFT methods, this last value is close to the E_i value 2.0 eV/nm^2 in Ref. [17], where the metastable state has presumably been obtained since no initial shift δz was considered. Even if the energy difference per nm^2 is small between the metastable state and the ground state, it has to be integrated on the total area of the interface to appreciate the respective stability.

Equally important is the energy barrier between the two states and, more precisely, the saddle point of the surface energy in configuration space. First, eight intermediate configurations have been constructed by linear interpolation between the two minima and thus corresponding to intermediate grain shifts $\delta z = n$ pm of the two crystalline grains. Second, DIIS calculations (direct inversion of iterative subspace [31]) have been performed with BigDFT code for a geometry optimization [32] of each of these initial configurations. Here, DIIS calculations correspond to structures relaxations toward close stationary points of the energy surface, usually minima but also saddle points. Indeed, all configurations have converged toward one or the other previous minima, except for the initial $\delta z = 3$ pm, which has led to a saddle point at 0.14 eV/nm^2 above the lowest minimum and a final shift $\delta z = 3.1 \pm 0.1$ pm. See in Fig. S14 (Supplemental Material [30]) the atomic configuration and its unstable direction along

which the energy second derivative is negative. The energy and the final shift δz of the saddle-point configuration are also plotted in Fig. 2.

IV. LDA EXCHANGE-CORRELATION FUNCTIONAL

We test here the strength of our results with respect to the choice of the exchange-correlation functional, which is the key approximation in any DFT calculations. Like PBE, the local density approximation (LDA) is also a standard choice for compound calculations. It usually results in an underestimation of the experimental lattice parameters by a few percent. The lattice parameters calculated with LDA are also lower than those obtained with PBE, and somehow LDA and PBE give the extreme values of the DFT results [28]. For this reason, we have also tested the characteristics of the IDB, when calculated with the LDA functional.

Except for the functional change, the GaN wurtzite lattice parameters have been determined with the same calculation parameters as above and we find: $a_{LDA} = 306.4$ pm, $c_{LDA} = 499.8$ pm, and $u_{LDA} = 0.377$ (see also Table S1 in the Supplemental Material [30]). Parameters a_{LDA} and c_{LDA} are indeed a few percent lower than both the PBE and the experimental results.

Starting now with the lattice structure corresponding to LDA and repeating the above protocol to build and relax the configurations containing the IDB defects, we obtain again two minima and one barrier. The shifts δz_{LDA} equal 8.2 ± 0.1 pm, -0.8 ± 0.1 pm, and 3.0 ± 0.1 pm, respectively, for the ground state, the metastable state, and the barrier (compare Fig. 4 and Fig. S9 in the Supplemental Material [30]). Similarly to the PBE result, we found an energy barrier above the ground state of 0.14 eV/nm^2. However we found higher defect energies at the minima than for PBE: 3.38 eV/nm^2 and 3.43 eV/nm^2. The fact that two different and well established exchange-correlation functionals both lead to double minima for the IDB, and especially a ground state with a shift δz in agreement with the experiment, reinforces our conclusions.

V. BOUNDARY CONDITIONS—ELECTROSTATIC EFFECTS

To assess the role of the boundary conditions on our results, calculations with free boundary conditions have also been carried out with the PBE functional. Instead of the two interacting IDB—due to the artificial periodicity perpendicular to the interfaces—there are now possible interactions between one IDB and the free surfaces parallel to it (configurations shown in Figs. S12 and S13 in the Supplemental Material [30]). The initial surfaces have been obtained by truncating the lattice perpendicularly to the [1 $\bar{1}$ 0 0] direction and are therefore nonpolar [24] (see Fig. S10 in the Supplemental Material [30]). No external atoms have been added at these (1 $\bar{1}$ 0 0) surfaces to passivate them, in order to get the clean-surface effects. All the atoms have been allowed to relax. The calculated relaxations of these bare surfaces are in agreement with those of previous studies [20,33–36], with a contraction and a rotation of the Ga-N bonds at the surface, the Ga atoms being displaced inward (see also Table S2 and Fig. S11 in the Supplemental Material [30]). For all configurations studied

from 32 atoms up to 128 atoms, the IDB has two stable configurations. The domains are shifted by $\delta z = 8$ pm in those with the lowest energy and by -1 pm in the metastable ones. These results are in agreement with those obtained above with periodic boundary conditions and thus with the experimental results.

Because of the IDB interactions and the resulting strain, we have seen above that the ideal domain separation at the IDB, or equivalently the shift δx to the crystalline interplanar distance $d_{1\bar{1}00}$, is more difficult to precisely determine [37] than the shift δz. Moreover, with free surfaces parallel to the IDB, we don't have the computer box periodicity to fix the total length of the configuration along x, and we can't plot energy curves like in Fig. 2. Thus, to carefully measure δx, we introduce a phase method where the atomic positions are compared to a reference crystal. This method is analog to the calculation of the hull function describing atomic displacements when two incommensurate structures are interacting [18]. It is also similar to the geometrical phase analysis [38–40], used in high resolution electron microscopy to measure displacement and strain fields in materials. In this last method however, inputs are images and the variation from a lattice reference is processed through Fourier space. When data are atomic coordinates given by computations, an atomic phase can be simply calculated for each atom ℓ as $\Phi_\ell = 2\pi(\mathbf{r}_\ell \cdot \mathbf{q} \mod 1)$, where $\mathbf{q}$ is a chosen reciprocal vector of the reference lattice and $\mathbf{r}_\ell$ is the position of atom ℓ. Here, to get the atomic displacements in length unit along direction $\mathbf{q}$, we plot $\Delta_\ell = \mathbf{u}_\ell \mod (1/\|\mathbf{q}\|)$ versus $\mathbf{u}_\ell = \mathbf{r}_\ell \cdot \mathbf{q}/\|\mathbf{q}\|$. Note that $1/\|\mathbf{q}\|$ is the interplanar distance corresponding to $\mathbf{q}$. Thus, the atomic phases and the atomic shifts associated with $\mathbf{q}$ are related by $\Phi_\ell = \Delta_\ell 2\pi/\|\mathbf{q}\|$.

In our particular case, the value δx as well as the elastic strain in the crystal grains can be extracted from the plot associated with $\|\mathbf{q}\| = 2/b$ in the x direction. This is shown in Fig. 3 for the periodic system and for the system with free surfaces. In both cases the crystalline grains are in tension. However, the strain ε_{xx} is three times larger in the free-surface case, and thus the mixed interactions between surfaces and IDB are larger than the interactions between the IDB themselves. We have not enough results to deduce the variations of ε_{xx} versus distances, but we have indeed checked the logical result that it decreases with the system sizes. With surfaces, we found a larger grain shift δx than with periodic conditions (see also Fig. S5 in the Supplemental Material [30]). Taking into account that these systems are under a larger stress, the periodic boundary conditions give a more reliable result. We can conclude that the domain shift δx is close to zero. This is indeed in agreement with the experimental results of Ref. [2] where it is concluded from the value of their error bar that $\delta x < 4$ pm. Note however that the value δx obtained with free surfaces is due to electrostatic interactions between the IDB and the free surfaces and thus, could be present in thin nanowires where IDB can be close to the surface [8,9].

VI. CONCLUSION

Several experimental techniques are under development to reach the picometer resolution and to study extended defects, especially in semiconductors where they play an important
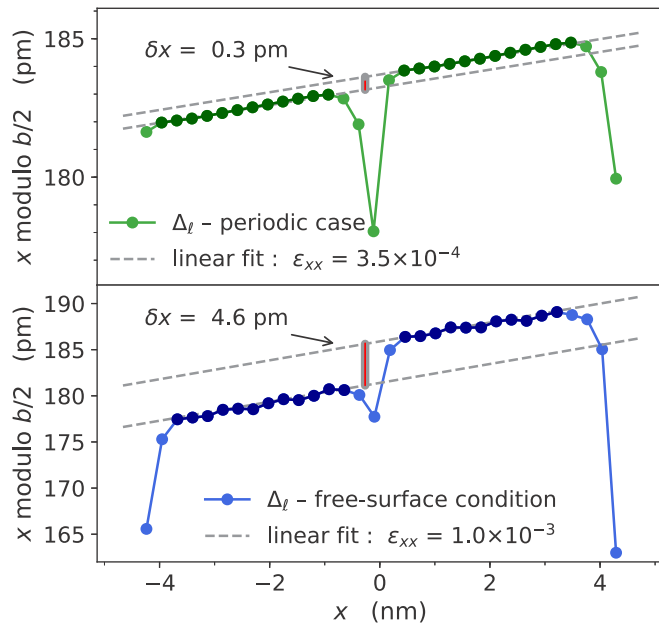
FIG. 3. Atomic shift Δ_ℓ associated with the interplane distance $b/2$ in the direction x, i.e., [$1\bar{1}0\,0$]. The atomic configurations have 128 atoms. *Top:* two IDB with periodic boundary conditions. *Bottom:* one IDB and two free surfaces. The plots are centered on a IDB and the vertical origins are arbitrary. The grain shift δx and the strain ε_{xx} are extracted from the linear interpolations through the data of each domain (darker disks). One Ga xy layer is used in the calculation. The deviating values of Δ_ℓ in the middle and at the extremities correspond to the atomic relaxations at the IDB and at the free surfaces.

role on the physical properties of electronic and optoelectronic devices. These techniques are mostly based on the interference of coherent x-ray [2,41] and electron diffraction [42] beams, or on the scanning of transmitted electron beam by correcting both spherical aberrations and distortions [7,43]. As in the calculation, they require a portion of good crystal to provide a reference in order to estimate the lattice displacements induced by the presence of extended defects.

In parallel to these experimental works, *ab initio* calculations should now attempt to reach a similar goal to enable cross-talks between experiment and theory. Along this line, we have revisited here the theoretical basis of IDB*, focusing on the detail of its structure, and this resolution can indeed be reached in gallium nitride. To achieve this accuracy, which is validated by experimental results, we have taken advantage of the high precision achieved by the DFT code [22] and by a favorable behavior of simulations for the GaN compound. The high precision of the calculations comes from different characteristics of the program, in particular the type of wavelet basis and their implementation [21]. The mark of these ingredients is the regularity of the energy and phase curves (Figs. 2 and 3) with subpicometer input variations (see also Fig. S5 in the Supplemental Material [30]).

For the well-established IDB* structure, we found that the GaN inversion domains are subjected to a positive or a negative extra lattice shift parallel to the hexagonal axis leading to two states, respectively, IDB$^+$ and IDB$^-$. The positive shift δz leads to the ground state and its value of 8 pm is in agreement
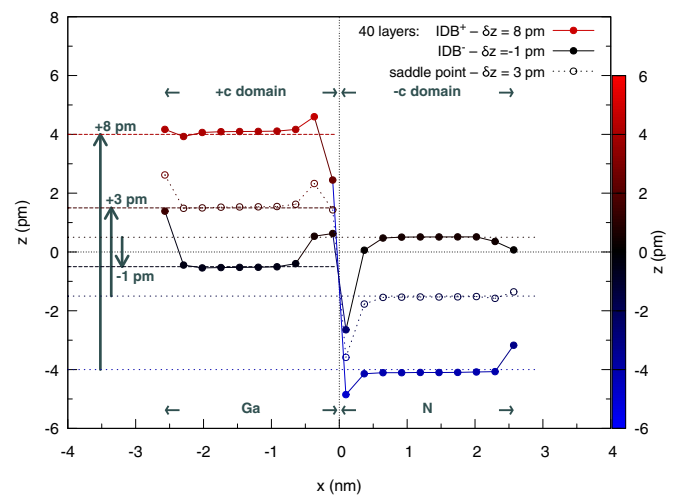

FIG. 4. Atomic coordinate z along the hexagonal axis [0 0 0 1] versus the position x along [$1\,\bar{1}\,0\,0$], i.e., perpendicular to the interface. One atomic layer crossing orthogonally the interface is considered for this graph. It consists of Ga atoms on one side ($+c$ domain) and N atoms on the other side ($-c$ domain). The results are for three 80-atom configurations (i.e., with 40 layers parallel to the IDB): the ground state IDB$^+$, the metastable state IDB$^-$, and the saddle-point state. They correspond, respectively, to domain shifts δz equal to $+8.2$ pm, -1.0 pm, and $+3.1$ pm.

with the reported experimental results [2]. We have carefully checked the effects of the boundary conditions. Like the size of the configurations, they do not change the ground state status of the two minima, neither their respective values of δz. Note that in simulations with Tersoff-Brenner potentials for GaN, i.e., without electronic density taken into account, only one minimum had been found [2]. GaN wurtzite is a strongly polarized compound and we could expect a similar behavior for IDB in wurtzite ZnO, which has very similar physical properties.
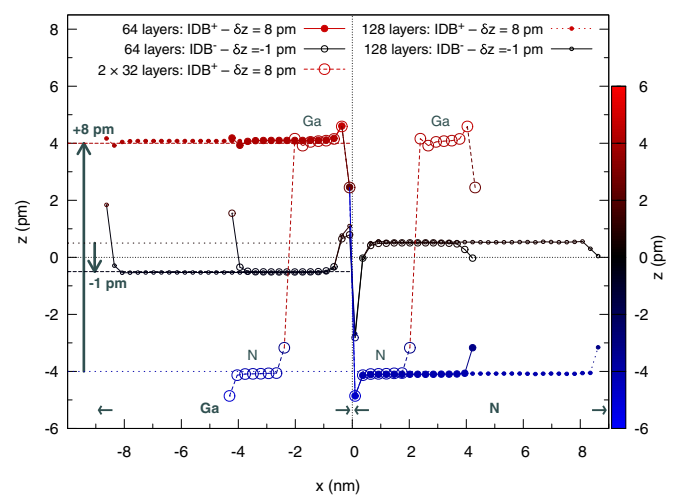

FIG. 5. Summary of the results for 128-atom and 256-atom configurations (64 and 128 layers, respectively) showing the atomic coordinate z along the hexagonal axis versus the position x perpendicular to the interface. One special configuration contains four instead of two IDB (2×32 layers) and thus four domains. The coherence of the results among different system sizes is thus validated.

While our various calculations of δz converge, the domain shift δx, perpendicular to the interface, is more dependent on the boundary conditions. The interactions between surface and IDB are strong for the configuration sizes studied here, and periodic conditions are recommended, as usual, for this determination. Nevertheless, for thin wires grown by molecular beam epitaxy where IDB can be located very close to the surface, our results with free-surface conditions can be pertinent and predict larger values of δx than in the bulk. Determined with periodic conditions, the shift δx for the bulk is lower than half a picometer. Experimentally, this value is difficult to measure too, but the interval given [2] of $\delta x <$ 4 pm is in agreement with our result.

ACKNOWLEDGMENTS

APPENDIX: GRAIN SHIFT δz

The grain shift δz is the main quantity of the system that indicates a discrepancy between the original IDB* model [14] and our calculation, as well as with the experimental results [2]. It is therefore crucial to calculate it carefully. This could be done by using the phase method introduced above. Indeed, in the same way as the shift δx has been calculated, we could calculate δz using the c-lattice parameter instead of the b one, i.e., with $\Delta_\ell = z_\ell \mod c/2$. However in an atomic row perpendicular to the IDB, the coordinate z varies by a much lower quantity than $c/2$. Thus plotting z_ℓ versus x is enough to determine δz.

Figure 4 shows the atomic coordinates z_ℓ, as well as the global shifts δz found for three states: the ground-state IDB$^+$, the metastable state IDB$^-$, and the saddle-point state separating IDB$^+$ and IDB$^-$. This figure and Fig. 5 show the precision achieved by the calculations and the consistency of the results with the system size. More generally, Figs. 3 and 4 show the atomic relaxations at the interface, respectively, along x and z. No relaxation occurs along y.

[1] K. Lejaeghere, G. Bihlmayer, T. Bjoerkman, P. Blaha, S. Bluegel, V. Blum, D. Caliste, I. E. Castelli, S. J. Clark, A. Dal Corso, S. de Gironcoli, T. Deutsch, J. K. Dewhurst, I. Di Marco, C. Draxl, M. Dulak, O. Eriksson, J. A. Flores-Livas, K. F. Garrity, L. Genovese *et al.*, Reproducibility in density functional theory calculations of solids, Science **351**, aad3000 (2016).

[2] S. Labat, M.-I. Richard, M. Dupraz, M. Gailhanou, G. Beutier, M. Verdier, F. Mastropietro, T. W. Cornelius, T. U. Schülli, J. Eymery, and O. Thomas, Inversion domain boundaries in GaN wires revealed by coherent bragg imaging, ACS Nano **9**, 9210 (2015).

[3] L. T. Romano, J. E. Northrup, and M. A. O'Keefe, Inversion domains in GaN grown on sapphire, Appl. Phys. Lett. **69**, 2394 (1996).

[4] J. L. Rouvière, M. Arlery, B. Daudin, G. Feuillet, and O. Briot, Transmission electron microscopy structural characterisation of GaN layers grown on (0001) sapphire, Mater. Sci. Eng. B **50**, 61 (1997).

[5] J.-L. Rouvière, M. Arlery, and A. Bourret, Structural characterisation of GaN layers: influence of polarity and strain release, Inst. Phys. Conf. Ser. **157**, 173 (1997).

[6] A. M. Sanchez, G. Nouet, P. Ruterana, F. J. Pacheco, S. I. Molina, and R. Garcia, A mechanism for the multiple atomic configurations of inversion domain boundaries in GaN layers grown on Si(111), Appl. Phys. Lett. **79**, 3588 (2001).

[7] F. Liu, R. Collazo, S. Mita, Z. Sitar, S. J. Pennycook, and G. Duscher, Direct observation of inversion domain boundaries of GaN on c-sapphire at sub-Ångstrom resolution, Adv. Mater. **20**, 2162 (2008).

[8] X. J. Chen, G. Perillat-Merceroz, D. Sam-Giao, C. Durand, and J. Eymery, Homoepitaxial growth of catalyst-free GaN wires on N-polar substrates, Appl. Phys. Lett. **97**, 151909 (2010).

[9] T. Auzelle, B. Haas, M. Den Hertog, J.-L. Rouvière, B. Daudin, and B. Gayral, Attribution of the 3.45 eV GaN nanowires luminescence to inversion domain boundaries, Appl. Phys. Lett. **107**, 051904 (2015).

[10] A. Chowdhury, H. M. Ng, M. Bhardwaj, and N. G. Weimann, Second-harmonic generation in periodically poled GaN, Appl. Phys. Lett. **83**, 1077 (2003).

[11] J. Hite, M. Twigg, M. Mastro, J. Freitas, J. Meyer, I. Vurgaftman, S. O'Connor, N. Condon, F. Kub, S. Bowman, and C. Eddy, Development of periodically oriented gallium nitride for non-linear optics, Opt. Mater. Express **2**, 1203 (2012).

[12] J. K. Hite, N. Y. Garces, R. Goswami, M. A. Mastro, F. J. Kub, and C. R. Eddy, Jr., Selective switching of GaN polarity on Ga-polar GaN using atomic layer deposited Al$_2$O$_3$, Appl. Phys. Express **7**, 025502 (2014).

[13] J. L. Rouvière, M. Arlery, R. Niebuhr, K. H. Bachem, and O. Briot, Transmission electron microscopy characterization of GaN layers grown by MOCVD on sapphire, Mater. Sci. Eng. B **43**, 161 (1997), e-MRS 1996 Spring Meeting, Symposium C: UV, Blue and Green Light Emission from Semi-conductor Materials.

[14] J. E. Northrup, J. Neugebauer, and L. T. Romano, Inversion Domain and Stacking Mismatch Boundaries in GaN, Phys. Rev. Lett. **77**, 103 (1996).

[15] P. J. Schuck, M. D. Mason, R. D. Grober, O. Ambacher, A. P. Lima, C. Miskys, R. Dimitrov, and M. Stutzmann, Spatially resolved photoluminescence of inversion domain boundaries in GaN-based lateral polarity heterostructures, Appl. Phys. Lett. **79**, 952 (2001).

[16] R. Kirste, R. Collazo, G. Callsen, M. R. Wagner, T. Kure, J. Sebastian Reparaz, S. Mita, J. Xie, A. Rice, J. Tweedie, Z. Sitar, and A. Hoffmann, Temperature dependent photoluminescence of lateral polarity junctions of metal organic chemical vapor deposition grown GaN, J. Appl. Phys. **110**, 093503 (2011).

[17] V. Fiorentini, Origin of the efficient light emission from inversion domain boundaries in GaN, Appl. Phys. Lett. **82**, 1182 (2003).

[18] A. Gautam, C. Ophus, F. Lançon, V. Radmilovic, and U. Dahmen, Atomic structure characterization of an incommensurate grain boundary, Acta Materialia **61**, 5078 (2013).

[19] M. Leszczynski, H. Teisseyre, T. Suski, I. Grzegory, M. Bockowski, J. Jun, S. Porowski, K. Pakula, J. M. Baranowski, C. T. Foxon, and T. S. Cheng, Lattice parameters of gallium nitride, Appl. Phys. Lett. **69**, 73 (1996).

[20] J. Zúñiga Pérez, V. Consonni, L. Lymperakis, X. Kong, A. Trampert, S. Fernández-Garrido, O. Brandt, H. Renevier, S. Keller, K. Hestroffer, M. R. Wagner, J. S. Reparaz, F. Akyol, S. Rajan, S. Rennesson, T. Palacios, and G. Feuillet, Polarity in GaN and ZnO: Theory, measurement, growth, and devices, Appl. Phys. Rev. **3**, 041303 (2016).

[21] L. Genovese, A. Neelov, S. Goedecker, T. Deutsch, S. A. Ghasemi, A. Willand, D. Caliste, O. Zilberberg, M. Rayson, A. Bergman, and R. Schneider, Daubechies wavelets as a basis set for density functional pseudopotential calculations, J. Chem. Phys. **129**, 014109 (2008).

[22] BigDFT, version 1.8 (2016).

[23] A. Cerioni, L. Genovese, A. Mirone, and V. A. Sole, Efficient and accurate solver of the three-dimensional screened and unscreened poisson's equation with generic boundary conditions, J. Chem. Phys. **137**, 134108 (2012).

[24] V. M. Bermudez, The fundamental surface science of wurtzite gallium nitride, Surf. Sci. Rep. **72**, 147 (2017).

[25] S. Goedecker, M. Teter, and J. Hutter, Separable dual-space gaussian pseudopotentials, Phys. Rev. B **54**, 1703 (1996).

[26] C. Hartwigsen, S. Goedecker, and J. Hutter, Relativistic separable dual-space Gaussian pseudopotentials from H to Rn, Phys. Rev. B **58**, 3641 (1998).

[27] J. P. Perdew, K. Burke, and M. Ernzerhof, Generalized Gradient Approximation Made Simple, Phys. Rev. Lett. **77**, 3865 (1996).

[28] P. Haas, F. Tran, and P. Blaha, Calculation of the lattice constant of solids with semilocal functionals, Phys. Rev. B **79**, 085104 (2009).

[29] L. Genovese and T. Deutsch, Multipole-preserving quadratures for the discretization of functions in real-space electronic structure calculations, Phys. Chem. Chem. Phys. **17**, 31582 (2015).

[30] See Supplemental Material at http://link.aps.org/supplemental/10.1103/PhysRevB.98.165306 for a file `IDB-supplement-2018.pdf` with the following information: (1) k-point grid and h-grid parameter convergences; (2) lattice parameter determinations; (3) grain-shift δx convergence; (4) plots of the atomic configuration and the electron density of IDB$^+$; (5) grain-shift δz with LDA; (6) surface relaxation; (7) collection of ball-and-stick models; (8) list and description of the atomic-configuration files also available as Supplemental Material.

[31] F. Eckert, P. Pulay, and H.-J. Werner, Ab initio geometry optimization for large molecules, J. Comput. Chem. **18**, 1473 (1997).

[32] E. Machado-Charry, L. K. Béland, D. Caliste, L. Genovese, T. Deutsch, N. Mousseau, and P. Pochet, Optimized energy landscape exploration using the ab initio based activation-relaxation technique, J. Chem. Phys. **135**, 034102 (2011).

[33] J. E. Northrup and J. Neugebauer, Theory of GaN(10$\bar{1}$0) and (11$\bar{2}$0) surfaces, Phys. Rev. B **53**, R10477 (1996).

[34] A. Filippetti, V. Fiorentini, G. Cappellini, and A. Bosin, Anomalous relaxations and chemical trends at III-V semiconductor nitride nonpolar surfaces, Phys. Rev. B **59**, 8026 (1999).

[35] M.-H Tsai, O. F Sankey, K. E Schmidt, and I. S. T. Tsong, Electronic structures of polar and nonpolar GaN surfaces, Mater. Sci. Eng. B **88**, 40 (2002).

[36] D. Segev and C. G. Van de Walle, Surface reconstructions on InN and GaN polar and nonpolar surfaces, Surf. Sci. **601**, L15 (2007).

[37] S. Goedecker, F. Lançon, and T. Deutsch, Linear scaling relaxation of the atomic positions in nanostructures, Phys. Rev. B **64**, 161102 (2001).

[38] M. Takeda and J. Suzuki, Crystallographic heterodyne phase detection for highly sensitive lattice-distortion measurements, J. Opt. Soc. Am. A **13**, 1495 (1996).

[39] M. J. Hÿtch, E. Snoeck, and R. Kilaas, Quantitative measurement of displacement and strain fields from HREM micrographs, Ultramicroscopy **74**, 131 (1998).

[40] J. L. Rouvière and E. Sarigiannidou, Theoretical discussions on the geometrical phase analysis, Ultramicroscopy **106**, 1 (2005).

[41] S. J. Leake, V. Favre-Nicolin, E. Zatterin, M.-I. Richard, S. Fernandez, G. Chahine, T. Zhou, P. Boesecke, H. Djazouli, and T. U. Schülli, Coherent nanoscale X-ray probe for crystal interrogation at ID01, ESRF – the European Synchrotron, Materials and Design **119**, 470 (2017).

[42] L. Wu, Y. Zhu, and J. Tafto, Picometer Accuracy in Measuring Lattice Displacements Across Planar Faults by Interferometry in Coherent Electron Diffraction, Phys. Rev. Lett. **85**, 5126 (2000).

[43] S. Ning, T. Fujita, A. Nie, Z. Wang, X. Xu, J. Chen, M. Chen, S. Yao, and T.-Y. Zhang, Scanning distortion correction in STEM images, Ultramicroscopy **184**, 274 (2018).